

Sample variance and Lyman- α forest transmission statistics

E. Rollinde¹, T. Theuns^{2,3}, J. Schaye⁴, I. Pâris¹, P. Petitjean¹

¹ UPMC Université Paris 06, UMR7095, Institut d'Astrophysique de Paris, F-75014, Paris, France

² Institute of Computational Cosmology, Department of Physics, University of Durham, Science Laboratories, South Road, Durham DH13LE

³ Universiteit Antwerpen, Campus Groenenborger, Groenenborgerlaan 171, B-2020 Antwerpen, Belgium

⁴ Leiden Observatory, Leiden University, P.O. Box 9513, 2300 RA Leiden, The Netherlands

21 February 2022

ABSTRACT

We compare the observed probability distribution function of the transmission in the H I Lyman- α forest, measured from the UVES ‘Large Programme’ sample at redshifts $z = [2, 2.5, 3]$, to results from the GIMIC cosmological simulations. Our measured values for the mean transmission and its PDF are in good agreement with published results. Errors on statistics measured from high-resolution data are typically estimated using bootstrap or jack-knife resampling techniques after splitting the spectra into chunks. We demonstrate that these methods tend to underestimate the sample variance unless the chunk size is much larger than is commonly the case. We therefore estimate the sample variance from the simulations. We conclude that observed and simulated transmission statistics are in good agreement, in particular, we do not require the temperature-density relation to be ‘inverted’.

Key words: cosmology: theory — methods: numerical — galaxies: intergalactic medium

1 INTRODUCTION

At high redshift, the intergalactic medium (IGM) contains the majority of baryons in the Universe (Petitjean et al. 1993; Fukugita et al. 1998), is highly ionised by the UV-background (UVB) produced by galaxies and QSOs (Gunn & Peterson 1965) at least since redshift $z \sim 6$ (Fan et al. 2006; Becker et al. 2007), becoming increasingly neutral near $z \sim 7$ (Mortlock et al. 2011). It is detected in absorption against bright sources as the H I Lyman- α forest (Lynds 1971); see Rauch (1998) for a review.

High signal-to-noise observations with high-resolution, echelle spectrographs such as the Ultraviolet and Visual Echelle Spectrograph (UVES) on the *Very Large Telescope* (VLT, e.g. Bergeron et al. 2004) and HIRES on Keck (e.g. Hu et al. 1995), of this forest of H I absorption lines, together with numerical simulations (Cen et al. 1994; Petitjean et al. 1995; Hernquist et al. 1996; Zhang et al. 1995; Theuns et al. 1998) and theoretical models (Bi et al. 1992; Schaye 2001) have painted a picture in which low column-density H I absorption lines trace the filaments of the ‘cosmic web’, and high column-density absorption lines trace the surroundings of galaxies. Simulations that include self-shielding of the UVB reproduce the observed column density distribution over 10 orders of magnitude (Altay et al. 2011).

In this paradigm, the IGM as probed by the Lyman- α forest consists of mildly non-linear gas density fluctuations. The gas traces the dark matter, and is photo-ionised and photo-heated by the UV-background. Although metals are detected in the IGM (Cowie et al. 1995), even at low densities (e.g. Schaye et al. 2003; Aracil et al. 2004), stirring of the IGM due to feedback from

galaxies or AGN is probably not strongly affecting the vast majority of the baryons (e.g. Theuns et al. 2002; McDonald et al. 2005). This makes it possible to use Lyman- α observations to constrain cosmological parameters (McDonald & Miralda-Escudé 1999; Rollinde et al. 2003; Viel & Haehnelt 2006; McDonald et al. 2006), as well as to probe the density distribution around quasars and galaxies (Rollinde et al. 2005; Guimarães et al. 2007; Kim & Croft 2008).

Photo-heating of the low-density IGM introduces a near-power law relation between its temperature, T , and density, ρ , of the form $T = T_0 \Delta^{\gamma-1}$, where $\Delta \equiv \rho/\langle\rho\rangle$ (Hui & Gnedin 1997; Theuns et al. 1998). The evolution of T_0 and γ have been measured (Schaye et al. 2000; Ricotti et al. 2000; McDonald et al. 2001; Lidz et al. 2006; Becker et al. 2007; Lidz et al. 2010; Becker et al. 2011), and depends on the re-ionization history (e.g. Theuns et al. 2002; Hui & Haiman 2003) and the hardness of the UV-background. When the gas is strongly photo-heated after the re-ionization of H I and He II, T_0 increases and the gas becomes nearly isothermal, $\gamma \rightarrow 1$; asymptotically the balance between photo-heating and adiabatic cooling results in $T = T_0 \Delta^{1/1.7}$ and a slowly decreasing T_0 with redshift (Hui & Gnedin 1997; Theuns et al. 1998). The amplitude of the optically thin ionising background rate (Γ_{12}), the temperature of the IGM (characterised by T_0 and γ), and the amplitude of fluctuations (σ_8) together determine the net amount of absorption (Rauch et al. 1997; Theuns et al. 2002; Hui & Haiman 2003; Bolton et al. 2005; Fan et al. 2006; Faucher-Giguère et al. 2008), and the value inferred by compar-

ing to simulations is very close to that computed by summing over sources by Haardt & Madau (2001).

It is also possible to compare the full probability distribution function of the transmission (TPDF) between simulations and data, which could provide a more accurate characterisation of the UVB. Such an analysis was performed by Bolton et al. (2008) and Viel et al. (2009), who compared TPDFs computed from simulations to those measured from a large sample of high-resolution UVES spectra (Kim et al. 2007). They performed a standard χ^2 analysis and suggested that an ‘inverted’ $T - \rho$ relation, $\gamma < 1$, may be required to fit the data. A similar conclusion was reached by Becker et al. (2007) using Keck data and different theoretical optical depth distributions. Calura et al. (2012) have done the same analysis with additional quasars at $z \gtrsim 3$. Their new analysis favours a value of γ that is larger than what they found before, but is still slightly lower than one. From a theory point of view it is difficult to understand how an inverted temperature-density relation might arise: simulations that include spectral hardening computed with a full radiative transfer calculation (e.g. McQuinn et al. 2009; Bolton et al. 2009) do not result in $\gamma < 1$. If the IGM’s $T - \rho$ relation were indeed inverted, there may be missing physics in simulations of the Lyman- α forest (such as the impact of blazars as studied recently by Chang et al. 2011; Puchwein et al. 2011), which may impact other statistics such as the Lyman- α power spectrum (e.g. McQuinn et al. 2011) and cosmological constraints derived from that (e.g. Gratton et al. 2008; Boyarsky et al. 2009). Partly for this reason, Lyman- α forest constraints were not used by Komatsu et al. (2009) in their determination of cosmological parameters from WMAP and other data.

However, there are both numerical and observational difficulties in the characterisation of the absorption. Numerical issues were investigated in a paper by Tytler et al. (2009), who analysed the importance of large-scale modes in the determination of the TPDF in a numerical simulation. These authors showed that smaller simulation boxes predict, on average, more absorption for a given value of the imposed ionising background. The box size used in the analyses of Bolton et al. (2008) is 56 Mpc, which, according to Tytler et al. (2009) (their Table 12), decreases the amplitude of the TPDF by 1 to 5 per cent in the flux range used in the analysis (0.2 to 0.8) as compared to a bigger box of 76.8 Mpc. The difference could be up to 10 per cent for even larger simulations. Even so, Tytler et al. (2009) also found that the predicted TPDF (with their box size of 76.8 Mpc) differs from the observed one, although to a lesser extent than that seen by Bolton et al. (2008). They did not consider an inverted temperature-density relation, but discussed other plausible sources for the discrepancy: the lack of high column density lines ($\log_{10} N_{\text{HI}}(\text{cm}^{-2}) > 14$) in the simulation, unidentified metal lines, and the assumed mean flux values. Note that the last two issues were discussed and, at least partly, accounted for in Bolton et al. (2008).

However, an additional limitation, not considered in Tytler et al. (2009), is the relatively small number of observed high-resolution spectra. For example, Kim et al. (2007) use a sample of just 18 spectra. In this paper we use both simulations and data to get a better handle on just how well such a relatively small sample of spectra determines the TPDF.

We revisit the analysis of the transmission statistics in terms of its sample variance using four different observational determinations described below in Section 2.1: (i) the LUQAS sample of Kim et al. (2007) used by Bolton et al. (2008), (ii) the sample of Calura et al. (2012) that increases the number of quasar with

$z \gtrsim 3$, (iii) a sample of Keck spectra analysed and published by McDonald et al. (2000), and finally (iv) a UVES sample collected in the context of the ESO Large Programme ‘Cosmic Evolution of the IGM’ (Bergeron et al. 2004). We demonstrate that published errors on the mean transmission are often too small, they do not fully account for sample variance. The observed TPDFs are compared to mock spectra computed from a suite of hydrodynamical simulations called GIMIC (Crain et al. 2009, Section 2.3) that resolves both large and small scales by using ‘zoomed’ initial conditions. We generate many mock samples from GIMIC with the same redshift path as the observed samples, and use this to investigate sample variance in both the mean transmission and the transmission probability distribution. In particular, we show how strong lines, which are relatively rare, nevertheless have substantial impact on both the mean transmission and its probability distribution, something which Viel et al. (2004) commented on in the context of the transmission power spectrum. Given the small redshift paths of the data, we conclude that observations and simulations are mutually consistent, because of the relatively ‘large sample variance’.

2 OBSERVED AND SIMULATED LYMAN- α SPECTRA

2.1 Observed samples

The transmission in the Lyman- α forest is the ratio $F = F_o/C$ of the measured flux (F_o) over what the flux would be in the absence of absorption. Measuring F requires knowledge of the intrinsic flux of the quasar (C ; the ‘continuum’), and since we are only interested in absorption due to neutral hydrogen (HI Lyman- α , $n = 1 \rightarrow 2$, $\lambda_0 = 1215.57 \text{ \AA}$), we also need to know the contribution to the absorption from other elements (‘metals’). Neither the continuum nor the contribution from metals are easy to determine: the intrinsic QSO spectrum contains broad emission lines and, moreover, the combination of a narrow slit with an echelle spectrograph – required to obtain the high spectral resolution – means the spectra cannot be accurately flux calibrated. ‘Continuum fitting’ spectra to determine C then involves drawing a smooth curve connecting regions deemed free from absorption, a somewhat subjective procedure. Metal lines are eliminated by identifying lines too narrow to be due to hydrogen, or from line coincidences where a metal transition occurs at the same redshift as a (strong) HI absorber or other metal transition. Finally, a ‘proximity region’, *i.e.* the region close to the quasar where it dominates the UV-background, is excised.

Here we use four observational data sets to determine the mean transmission and its PDF, referred to below as the LP sample, the *LUQAS* sample, the sample of Calura et al. (2012), and the M00 sample.

- The LP sample is from our own independent analysis of a set of 18 UVES VLT spectra, collected as part of the European Southern Observatory’s ‘Large Programme’ (LP) ‘Cosmic Evolution of the intergalactic medium’ (Bergeron et al. 2004). These LP spectra have a high-resolution ($\lambda/\Delta\lambda \sim 45000$) and a high signal-to-noise ratio ($S/N \approx 25 - 30$ per pixel), and were re-binned on to 0.05 \AA pixels. The continuum was fitted using an automatic method described in Aracil et al. (2004), and metal lines were removed by eliminating contaminated regions. There are no damped Lyman- α absorbers in these lines of sight. We compute the TPDFs and the mean transmission over three relatively small redshift ranges, centred at $z \simeq 2$ ($1.88 < z < 2.37$), $z \simeq 2.5$ ($2.37 < z < 2.71$) and $z \simeq 3$ ($2.71 < z < 3.21$). The total number of data pixels in the LP spectra for each of the redshift bins is 139830, 65067 and 30800

(of which a fraction 74%, 85% and 100% are in common with the LUQAS sample described below). The corresponding absorption distances¹ are $\Delta X = 10.5, 5.8$ and 2.9 respectively.

- The LUQAS sample used by Bolton et al. (2008) and Viel et al. (2009) is described in detail by Kim et al. (2007), including details of their method of continuum fitting and metal line identification. They fit metal lines in the Lyman- α part of the spectrum using VPFIT (Carswell et al. 1987), then use this to reconstruct an HI spectrum without the identified metals, as in Theuns et al. (2002). We find that this method has a similar effect on the transmission distribution as the method we used. The LUQAS sample has 18 spectra, 14 of which are part of the LP sample. Pixels within the Lyman- α forest within a given redshift range are extracted and combined into a histogram. We will refer to these published values as the ‘LUQAS’ data. The transmission PDFs of Kim et al. (2007) are averaged over the same redshift ranges as the LP ones.

- The Calura et al. (2012) sample is used to investigate the TPDF at redshift $z \gtrsim 3$. Their results are split in two bins, $2.62 < z < 3.17$ and $3.17 < z < 3.72$. We consider the first bin only to be compared to the other determinations. The absorption distance in this bin, after removal of fourteen DLA and LLS regions, is about 4.5. We use their estimate of the TPDF without metals and LLS.

- The M00 sample is a set of 8 Keck HIRES spectra with resolution and signal-to-noise similar to the UVES data, and is described in McDonald et al. (2000), hereafter M00. They use slightly different redshift bins that do not cover our lowest redshift bin, and go up to $z = 4.43$. We will therefore only consider their two lower redshift bins: $2.09 < z < 2.67$ (33791 data pixels, $\Delta X \simeq 3.5$) and $2.67 < z < 3.39$ (31897 data pixels, $\Delta X \simeq 3.7$).

Noise and errors in the continuum fitting can make the transmission $F < 0$ or $F > 1$. To compute the PDF of the transmission for the LP sample, we use the same binning as used in the LUQAS and McDonald et al. (2000) analyses, *i.e.* bins of width 0.05 between $F = 0.025$ and $F = 0.975$, plus extra bins for those pixels with $F < 0.025$ and $F > 0.975$. The PDF is then normalised² such that the sum of all values in all bins equals 20. The full covariance matrix of errors on the PDF is estimated using the jack-knife technique described in Lidz et al. (2006), but applied to the flux, while they applied this technique to $\delta_f \equiv (F - \bar{F})/F$. Specifically, we estimate the PDF $P(F_i)$ from the full data sample, divide the data set into 30 different subgroups, then estimate the PDF of the data sample omitting each subgroup iteratively, $P_k(i)$. The variance $\sigma_{i,j}$ is then computed on the difference between $P(F_i)$ and $P_k(F_j)$: $\sigma_{i,j}^2 = \sum_{k=1}^{k=30} [P(F_i) - P_k(F_i)][P(F_j) - P_k(F_j)]$. For the other observations we use error bars taken from the corresponding references. We discuss below how errors can be more reliably estimated as the variance among mock GIMIC samples. Both estimates of errors are shown in Fig. 3, while Table 1 indicates the variance among mock GIMIC samples.

¹ The absorption distance $dX/dz \equiv (1+z)^2 (\Omega_m (1+z)^3 + \Omega_\Lambda)^{-1/2}$, and quoted numerical values of dX assume $\Omega_m = 0.25$ and $\Omega_\Lambda = 0.75$.

² Pixels with $F < 0$ or $F > 1$ are assigned to the first and last PDF bins respectively, but the number of values in each bin is divided by the same $\Delta F = 0.05$ bin width when normalising the histogram.

Table 1. The mean transmission PDF of 18 UVES Large Program (LP) QSOs, in three redshift bins ($1.88 < z < 2.37$, $2.37 < z < 2.71$ and $2.71 < z < 3.21$). The error is the 2σ variance among mock GIMIC samples with ensemble average mean transmission $\langle F \rangle = 0.86, 0.77$ and 0.71 , respectively.

F bin centre	$\langle z \rangle = 2.0$	PDF and its error $\langle z \rangle = 2.5$	$\langle z \rangle = 3.0$
0.00	0.6052 ± 0.0990	1.2092 ± 0.1840	1.6649 ± 0.4680
0.05	0.2004 ± 0.0390	0.4044 ± 0.0670	0.4466 ± 0.1520
0.10	0.1472 ± 0.0240	0.2734 ± 0.0390	0.3130 ± 0.0850
0.15	0.1471 ± 0.0220	0.2211 ± 0.0300	0.2894 ± 0.0700
0.20	0.1380 ± 0.0220	0.1823 ± 0.0320	0.2441 ± 0.0690
0.25	0.1370 ± 0.0210	0.2253 ± 0.0290	0.2690 ± 0.0680
0.30	0.1383 ± 0.0220	0.2228 ± 0.0300	0.2468 ± 0.0660
0.35	0.1350 ± 0.0230	0.2062 ± 0.0310	0.2527 ± 0.0620
0.40	0.1539 ± 0.0240	0.2291 ± 0.0310	0.2423 ± 0.0660
0.45	0.1602 ± 0.0260	0.2797 ± 0.0350	0.2568 ± 0.0670
0.50	0.1815 ± 0.0270	0.2780 ± 0.0340	0.2745 ± 0.0670
0.55	0.2029 ± 0.0280	0.2877 ± 0.0340	0.3474 ± 0.0750
0.60	0.2253 ± 0.0290	0.3514 ± 0.0360	0.4180 ± 0.0810
0.65	0.2855 ± 0.0320	0.3899 ± 0.0380	0.5014 ± 0.0930
0.70	0.3341 ± 0.0370	0.4519 ± 0.0420	0.5879 ± 0.0980
0.75	0.4120 ± 0.0410	0.5815 ± 0.0520	0.7192 ± 0.1210
0.80	0.5508 ± 0.0480	0.8224 ± 0.0650	0.8886 ± 0.1390
0.85	0.8279 ± 0.0610	1.1295 ± 0.0850	1.3261 ± 0.1840
0.90	1.3857 ± 0.0810	1.7072 ± 0.1070	1.8837 ± 0.2460
0.95	3.5231 ± 0.1240	3.1205 ± 0.1760	2.9413 ± 0.4360
1.00	10.1090 ± 0.4230	7.4264 ± 0.4510	5.8861 ± 0.8010

2.2 Inconsistency between measured values of the mean transmission

We compare estimates of the mean transmission collected from the literature (McDonald et al. 2000; Kirkman et al. 2005; Kim et al. 2007; Faucher-Giguère et al. 2008), as well as measured by us for the LP sample. Errors are based on a bootstrap procedure, by re-sampling chunks of spectra of size 5\AA , or on the variance among chunks of the same size (Faucher-Giguère et al. 2008, hereafter FG). Kim et al. (2007) only provide errors on the effective optical depth, for a smaller bin in redshift $dz = 0.2$. We quote the corresponding errors on the flux $\sigma_F = F \sigma_\tau$, and we compute bootstrap errors for the LP using the same bins in redshift. Estimates from LP and LUQAS are given in Table 2 (upper rows), with corresponding 2σ errors, scaled to the same absorption distance.

The mean transmission values obtained from the LUQAS and LP samples differ by $2.13, 2.40$ and 2.75σ at $z = 2, 2.5$ and 3 , respectively (where σ is obtained from adding the bootstrap errors from both samples in quadrature). We recall that the LUQAS and LP samples are mostly based on the *same* raw data, but that those data were reduced by different groups. These differences must therefore be due to systematic errors in the adopted procedures, in particular differences in continuum fitting and the treatment of absorption from metals. Also, Kim et al. (2007) concluded that the treatment of the data, in particular continuum fitting, leads to notable differences between authors. Published values for \bar{F} from LUQAS, Kirkman et al. (2005) and FG agree within 1σ at $z = 2$, but the differences increase at higher z . The most discrepant values are 2.49σ at $z = 2.5$ (LUQAS versus McDonald et al. 2000, both are high-resolution data), and 3.9σ at $z=3$ (Kirkman et al. 2005, versus FG).

How reliable are the quoted errors? Kim et al. (2007) estimate errors on the effective optical depth, $-\ln(\bar{F})$, by bootstrapping the LUQAS spectra in chunks of 5\AA . They do not mention convergence tests with chunk size for the error on the mean flux, but they do note that a modified jack-knife method, using 50\AA chunks, yields errors that are too low – comparable to the estimated variance due to continuum placement alone. They nevertheless use jack-knife errors with 50\AA chunks to compute the variance of the transmission PDF. Calura et al. (2012) compare errors on the TPDF estimated with a bootstrap on 5\AA chunks and with a jack-knife on 50\AA chunks. They find similar results, but do not mention convergence tests with chunk size either. FG (2008) mention that “We have verified that the error estimates have converged for our choice of segment length”, but they do not present quantitative results.

Bootstrap errors depend on the arbitrary size of the chunks from which they are computed. Indeed, for the LP data at $z = 2.5$, we find variances in the mean flux of $\sigma = [0.25, 0.53, 0.78, 1.14, 1.03, 1.33, 1.15, 1.16] \times 10^{-2}$ for chunk sizes of $[0.2, 1, 5, 25, 50, 125, 250, 625]\text{\AA}$. Although σ converges for very large chunk sizes $\gtrsim 25\text{\AA}$, as expected, we suggest that typical published errors based on 5\AA chunks underestimate the variance by ~ 50 per cent. Note that the largest chunk size we tested, 625\AA , is comparable to the extent of the Lyman- α forest in a $z \sim 3$ QSO. We discuss the reliability of bootstrap errors using GIMIC mocks further in Section 2.4 below.

2.3 Mock samples

We use the GIMIC (Galaxies-Intergalactic Medium Interaction Calculation, Crain et al. 2009) simulations, a set of smoothed particle hydrodynamics simulations (SPH) of five nearly spherical regions of co-moving radius $R \sim 18h^{-1}\text{Mpc}$ picked from the Millennium simulation (Springel et al. 2005). The simulations have a gas particle mass of $1.4 \times 10^6 h^{-1} M_\odot$. These ‘zoomed’ simulations allow us to obtain high numerical resolution yet include the effects of large-scale power, *i.e.* the simulation probes a range of environments, from massive clusters to deep voids. The effect of large-scale structures, as discussed in Tytler et al. (2009), is thus accounted for.

The GIMIC simulations were performed with the GADGET-3 code, an evolution of GADGET-2 described last by Springel (2005), with modules for star formation, feedback from galactic winds, chemo-dynamics, and radiative cooling and photo-heating due to an imposed evolving UV-background, as described in Schaye & Dalla Vecchia (2008); Dalla Vecchia & Schaye (2008) and Wiersma et al. (2009b, a), respectively, see also Schaye et al. (2010). The assumed cosmological parameters are $(\Omega_{\text{cdm}} + \Omega_b, \Omega_\Lambda, \Omega_b, n_s, h, \sigma_8) = (0.25, 0.75, 0.045, 1, 0.9, 0.73, 0.9)$. The five GIMIC regions are picked such that their over-densities at redshift $z = 1.5$ are $(-2, -1, 0, 1, 2)$ times the root-mean-square deviation, σ , from the mean on the spatial scale of the spheres. Re-ionization of HI is assumed to occur at $z = 9$, heating the IGM to $T \sim 10^4\text{K}$, and of HeII at $z = 3.5$. As also shown by Wiersma et al. (2009b), the evolution of T_0 and γ in the simulations is broadly consistent with the Schaye et al. (2000) measurements, see also Fig. 1. For densities close to the mean, $\gamma \gtrsim 1.3$, and the temperature-density relation is never ‘inverted’.

We compute 1000 mock Lyman- α forest spectra by tracing straight lines through a cube³ embedded well within each of the

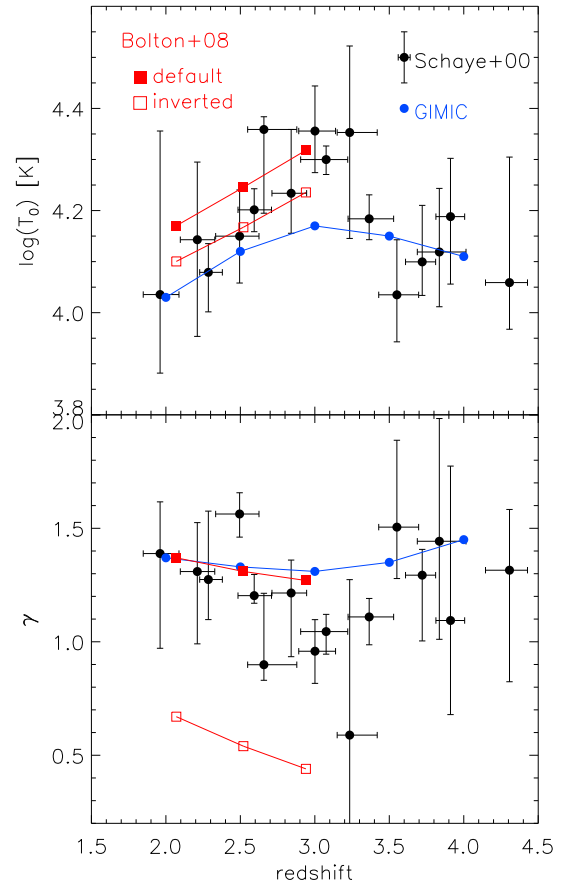


Figure 1. Evolution of the parameters T_0 and γ of the temperature-density relation $T = T_0 (\rho/\langle\rho\rangle)^{\gamma-1}$, as measured by Schaye et al. (2000, black circles with error bars) and in the GIMIC simulation (blue connected dots). The temperature-density relation in GIMIC is broadly consistent with the measured values. HeII re-ionization causes the rise in T_0 and the corresponding dip in γ in the GIMIC simulations at redshift $z \sim 3.2$, but γ never drops below ~ 1.3 . Red symbols are from the model of Bolton et al. (2008): filled squares are for their default model, open squares are for their model 20-256g3 that best fits the transmission PDF they inferred from LUQAS. This model has an inverted temperature-density relation, *i.e.* $\gamma < 1$.

five spheres, extracting density, temperature and peculiar velocity along them, and then computing the corresponding optical depth as described in Theuns et al. (1998). Crain et al. (2009) explain in their appendix how to combine results from individual spheres to correctly reproduce statistics valid for the full Millennium volume: we use the weights listed in their Table A1. Given these weights, we generate a ‘mock’ LP sample by randomly selecting spectra from each of the five spheres until the redshift path of mock and LP samples are the same. We repeat this procedure 400 times to obtain a ‘suite’ of mock samples. Note that every single mock sample in the

well away from the edges of the spheres to avoid artificial boundary effects, see Crighton et al. (2010) for details. We will call a Lyman- α spectrum obtained from a single cut through the cube a *short* spectrum.

³ The cubes have sides $\sim 11 h^{-1}$ co-moving Mpc which ensures we stay

suite has the same redshift path as the LP sample. Each spectrum is convolved with a Gaussian to match the UVES spectral resolution, re-binned to the UVES pixel size, and we add noise with similar statistical properties as measured in the observed spectra. Our results do not change significantly if we only use the GIMIC mean density sphere. We can compute flux statistics for a given mock sample simply from all pixels in all short spectra that make-up the mock sample. However, when computing bootstrap errors below, we combine these short spectra into a Lyman- α spectrum that mimics the full absorption distance of a given LP spectrum.

It is difficult to accurately mimic the effect of ‘continuum fitting’ as applied to observations to the simulated samples, because the wavelength range over which the observed continuum is supposed to vary is large compared to the size of an individual simulated spectrum. In the observations, the true and estimated continua are thought to differ by about 1–3 per cent (see e.g. Aracil et al. 2004; Faucher-Giguère et al. 2008). Therefore, to investigate plausible continuum uncertainties, we compare statistics from the original samples to those in which we multiply the flux by a constant factor of 1.02 to mimic a 2 per cent systematic offset between ‘true’ and ‘fitted’ continua.

The Lyman- α optical depth in a spectrum depends on the evolving photo-ionization rate,

$$\Gamma = 4\pi \int_{\nu_T}^{\infty} \frac{J(\nu)}{h\nu} \sigma_{\nu} d\nu \equiv \Gamma_{12} 10^{-12} \text{ s}^{-1}, \quad (1)$$

where $J(\nu)$ is the mean intensity of the ionising radiation at a given redshift, ν_T is the frequency of the Lyman limit, σ_{ν} is the hydrogen photo-ionization cross section. Within a suite of mock samples we use the same value for Γ_{12} , and will refer to the ‘ensemble average’ mean transmission of the suite as $\langle F \rangle$. The mean transmission, \bar{F} , of a given mock sample can differ significantly from the ensemble average $\langle F \rangle$ of the corresponding suite because of ‘sample variance’ and the same is true for its PDF. We estimate the sample variance in a given suite by comparing all 400 mock samples that make-up the suite. We emphasize that because the simulated samples keep probing the same density field, the real dispersion is likely to be larger than this estimate.

The value of the photo-ionization rate Γ_{12} is uncertain. Theuns et al. (1998) show that in the optically thin case, simulations can be run with one value for Γ_{12} and later accurately scaled to another value. To investigate the effect of uncertainties in Γ_{12} , we generate many suites of mock samples, with different values of Γ_{12} and hence of the ensemble average transmission, $\langle F \rangle$.

2.4 Estimates of errors with mock samples

We can check the reliability of the bootstrap errors discussed in Section 2.2 using GIMIC mock samples. We first examine whether mocks generated from the simulation give the same errors on the mean flux as observed samples when the errors are estimated in the same way. Faucher-Giguère et al. (2008) divide the variance σ_i of the mean flux measured along chunks of 3 Mpc proper size, by the square root of the number of chunks. They find $\sigma_i = [0.13, 0.11, 0.09]$ at $z = [3, 2.4, 2]$, with 193, 263 and 50 chunks respectively. Applying this procedure first to the LP data, we find $\sigma_i = [0.125, 0.13, 0.095]$ at $z = [3, 2.5, 2]$, with 37, 262 and 413 chunks respectively. Applied to our mocks we find $\sigma_i = [0.14, 0.14, 0.11]$. Therefore both our analysis of the LP observations, and of the GIMIC simulations, give error estimates in reasonable agreement with those obtained by Faucher-Giguère et al.

(2008). Kim et al. (2007) estimate errors on the effective optical depth, $-\ln(\bar{F})$, by bootstrapping the LUQAS spectra in chunks of size 5 Å. We concentrate on their estimate at $\bar{z} = 2.59$ with a bin in redshift of $\Delta z = 0.2$, corresponding to a velocity path of 88682 km s⁻¹. We use the GIMIC simulations to generate many mock versions of the LUQAS sample, each with the same velocity path, and estimate the variance σ for the same chunk size. The average value for our mocks is $\sigma_F = F \sigma_{\tau} = 0.0124$, identical to their bootstrap error. Finally, we compare errors estimated from GIMIC against our own bootstrap errors obtained from the LP data, as discussed in the previous section. At $z = 2.5$ and for a velocity path of ~ 190000 km s⁻¹, we calculate bootstrap variances of $\sigma = [0.26, 0.54, 0.80, 0.98, 1.22, 1.15] \times 10^{-2}$ for chunk sizes of $[0.2, 1, 5, 25, 125, 625]$ Å for the simulated mocks, as compared to $\sigma = [0.25, 0.53, 0.78, 1.14, 1.33, 1.16] \times 10^{-2}$ for the LP observational data. We conclude that errors computed from GIMIC mocks are in excellent agreement with published errors, as well as errors obtained by us from the LP data, when simulated and observed errors are calculated in the same way.

The bootstrap errors discussed above clearly depend on the value of the chunk size for which they are computed, both for the data and for the simulated spectra. They start to converge for relatively large chunk sizes of ~ 25 Å, although the convergence is not yet clearly reached. Using simulations we can also calculate the variance between different mock samples: simply generate many mock samples for a given simulation, each with the same redshift path as a given observed sample, and evaluate the variance between mock *samples*. This variance is $[0.55, 0.88, 1.7] \times 10^{-2}$ at redshifts $z = [2, 2.5, 3]$, as compared to bootstrap errors using 25 Å chunks of $[0.50, 0.98, 2.1] \times 10^{-2}$, in reasonable agreement. Given the dependence of the variance on chunk size for small chunks, we will use the variance between mock samples to characterise the expected level of scatter in the data and to investigate the consistency between simulation and data. We suggest that error estimates that we obtain from determining the variance between mocks, are more realistic than the published, observed bootstrap errors.

3 THE TRANSMISSION PDF

We have computed the transmission PDFs of the LP sample over the same small redshift ranges as used by Kim et al. (2007). Because these redshift ranges are relatively narrow, evolution over them can be safely neglected, and hence we simply use simulation snapshots at a single redshift ($z \simeq 2, 2.5$ and 3 for the three bins used by Kim et al. 2007) when comparing to the observed data.

3.1 Variance of the transmission PDF

Fig. 2 illustrates that continuum fitting quite noticeably affects the transmission PDF near $F \simeq 1$, and comparison to the over-plotted data also suggests that uncertainties in continuum placement can explain the large differences in the *observed* PDFs at $F \simeq 1$. Recall that we mimic the errors in continuum fitting by a systematic shift in the continuum (Section 2.2). Clearly, given these uncertainties, this part of the TPDF cannot constrain models robustly (see also Meiksin et al. 2001). Fortunately, the distribution of pixels with $F < 0.7$, say, is relatively insensitive to the error in the continuum placement for high-resolution spectra and can thus be used to constrain the mean transmitted flux.

The GIMIC simulations that best reproduce the observed transmission PDFs for $F < 0.7$ have ensemble averaged mean

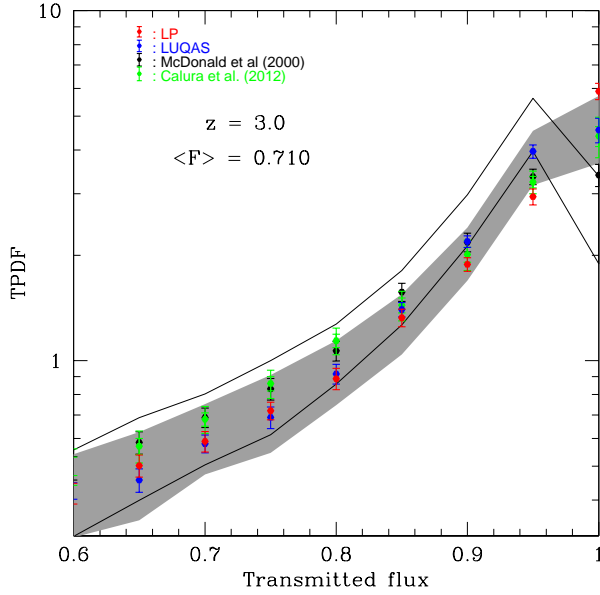


Figure 2. Effect of ‘continuum fitting’ the GIMIC simulations, *solid curves* show the 2σ range in the transmission PDFs of a sample of mocks with given ensemble averaged transmission, $\langle F \rangle$. When errors in continuum fitting are mimicked by a systematic shift in the continuum (see Section 2.2), the range is enclosed by full lines. Continuum fitting makes the shape of the TPDF uncertain close to $F = 1$. Note that we only show the range $0.6 \leq F \leq 1$. For $F < 0.6$, we find that the continuum correction is small compared to the 2σ range. Symbols with error bars are the data from the LP sample (red); LUQAS (blue), McDonald et al. (2000) (black) and Calura et al. (2012) (green). These also show significant differences in the range $F > 0.7$, plausibly due to the different continuum fitting methods applied in the data reduction.

transmissions of $\langle F \rangle = 0.86, 0.77$ and 0.71 at redshifts $z=2, 2.5$ and 3 , respectively, as discussed in more detail below. Observed and mock TPDFs with these values of $\langle F \rangle$, are compared at $z = 2, 2.5$ and 3 in Fig. 3. Light (dark) shaded regions show the 1σ and 2σ dispersion⁴ among TPDFs of this particular suite of mocks. There is considerable variance between the transmission PDFs of mock realisations, even though each mock realisation is generated from the same simulation with the full absorption distance of the LP observed sample.

The variance in the mocks increases with redshift since the redshift path decreases. The ratio of variance computed from GIMIC mock versus jack-knife variance is shown in Fig. 4. Except at $z = 2.5$, variance in mocks is systematically larger, from 10 to 50% at $z = 2$ and up to 100% at $z = 3$. Given that the simulations, if anything, *underestimate* sample variance, suggests once more that the observationally determined jack-knife errors are too small. Although more difficult to assess from other works, we found that the estimates of errors using the jack-knife method is very unstable given the relatively small size of the sample. We will therefore quote variances computed from our mocks only.

The LP and LUQAS data fall well within the 2σ region at all z for $F < 0.7$, with a possible exception of the $F \simeq 0$ bin at $z = 2$. It is possible that the latter discrepancy is due to the fact that simu-

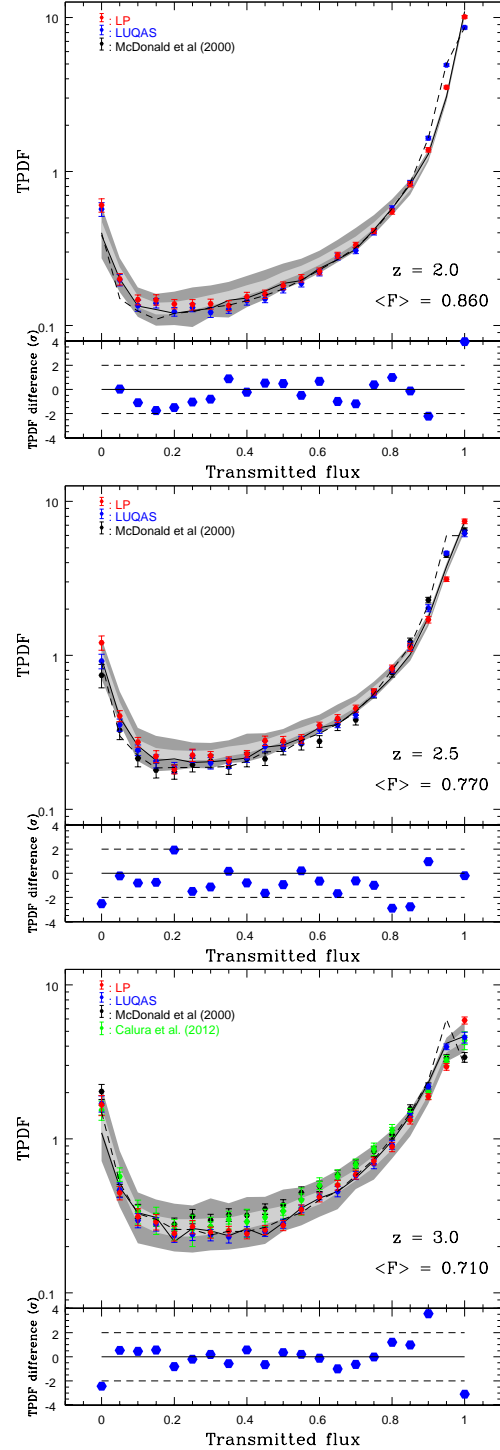


Figure 3. *Top to bottom:* PDF of the transmission at $z = 2, 2.5$ and 3 , of the best-fitting simulations (continuum fitted GIMIC simulation: *solid curve*; Bolton et al. 2008 model 20-256g3 shown as open squares in Fig 1: *dashed curve*), compared to observational data (symbols with error bars, LP sample: red; LUQAS: blue; Calura et al.: green; M00: $z=2.41$ and 3.0 , black). Error bars are 1σ jack-knife errors for LUQAS, LP and Calura et al., and bootstrap of 5\AA chunks for M00. Light (dark) shaded regions correspond to the 1 and 2σ range computed from 400 mock LP samples in GIMIC simulations with redshift and ensemble averaged mean transmission $\langle F \rangle$ as indicated in each panel. The simulations and various data sets agree well within the 2σ range at all three redshifts. Insets show (model-data)/ σ_o , where model is the best-fitting PDF for GIMIC, data and σ_o are the LP PDF and the variance estimated in GIMIC simulations. The GIMIC simulations fit the data for $F < 0.7$ even though $\gamma > 1$ at all z . For $F > 0.7$ and $z \leq 2.5$, different data sets are inconsistent and sensitive to continuum fitting (missing points are above 4).

⁴ They correspond to the 2.275, 15.8655, 84.13 and 97.725 percentiles computed from 400 realisations.

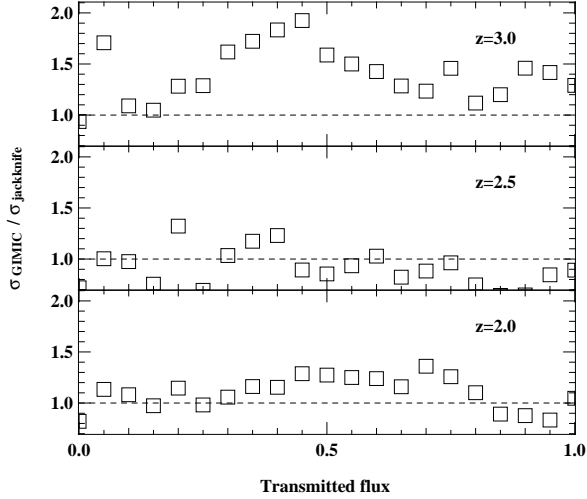


Figure 4. Ratio of PDF variance computed from GIMIC mocks to variance computed from jack-knife method for bins in transmitted flux in three different bins in redshift.

lations that assume the gas to be optically thin do not reproduce the observed number of strong lines (e.g. Tytler et al. 2009). Including self-shielding appears to solve this issue (Altay et al. 2011). The LP and LUQAS samples results are almost identical in bins where uncertainties in the position of the continuum does not interfere in the TPDF. They are also very similar to the results from Calura et al. (2012) sample that has one quasar in common (which makes one fourth of the total sample in this redshift bin). They also agree with results from McDonald et al. (2000) within the 2σ range estimated from the simulations.

The difference between the best-fitting simulated PDFs in GIMIC mock samples (among different values for Γ_{12} only) and our determination of the TPDF from the LP, divided by 1σ range on mock LP TPDF in GIMIC simulation, is shown in the bottom of each panel in Fig. 3. There is no evidence that the observed and simulated GIMIC PDFs are inconsistent at any redshift. The statistical interpretation of this measurement, and the derived constraints on the ionising background rate, are discussed further in Section 4.

3.2 Variance of the mean transmission

Interestingly, observations as well as simulations show large quasar-to-quasar variations in the mean transmission at a given redshift. To illustrate the origin of this large scatter, we analyse 400 mock samples from GIMIC generated with a given ensemble average, $\langle F \rangle = 0.79$, at redshift $z = 2.5$. The large scatter is due to strong absorption lines, which contribute significantly to the mean opacity: the small number of strong lines per QSO spectrum introduces the observed scatter, as we now show (see also Desjacques et al. 2007).

We have used a simple criterion to identify ‘lines’ in the spectrum as regions between two maxima in F ; we also demand that the corresponding minimum is sufficiently different from the lowest maximum to avoid identifying noise features as lines. More specifically, this algorithm identifies all local minima and maxima on a spectrum smoothed with a Gaussian kernel of width 8 km s^{-1} . A line consists of all pixels between two maxima that satisfy the following two conditions: (i) two successive maxima must be separated by more than 8 km s^{-1} and (ii) the flux difference between the maxima and the minimum they straddle must be larger than four

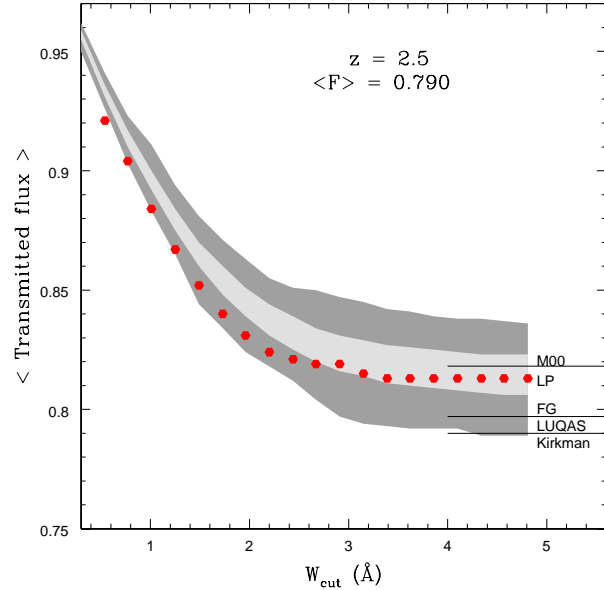


Figure 5. Mean transmission of spectra that include all lines with equivalent width $W < W_{\text{cut}}$ for the LP sample (red dots), and the corresponding 1 and 2σ range in this quantity estimated from GIMIC mock samples (grey and dark regions, respectively). The net mean transmission values, \bar{F} , for the LUQAS, M00, Faucher-Giguère et al. (2008; FG) and Kirkman et al. (2005) data are indicated by horizontal lines (FG and LUQAS values of \bar{F} are identical). There is significant scatter in \bar{F} of the GIMIC samples when $W_{\text{cut}} \gtrsim 1.5 \text{ Å}$, but as strong lines are excised, the dispersion decreases significantly. This shows that strong lines are mostly responsible for the scatter. The observed values of the net mean transmission, $\bar{F}(W < \infty)$, are well within the 2σ range estimated from the GIMIC simulations.

times the estimated error per pixel. Each pixel is then assigned to a line, with given equivalent width, W . We can now compute the mean transmission in a mock sample (or the LP data) for all pixels in lines with W less than some maximum equivalent width, W_{cut} .

The mean transmission, $\bar{F}(W_{\text{cut}})$, for all pixels in lines weaker than a given value of W_{cut} is plotted as a function of W_{cut} in Fig. 5 as red dots for the LP sample, with grey and dark regions the 1 and 2σ range estimated from the mock GIMIC samples. For a high cut in W , all pixels are used and $\bar{F}(W_{\text{cut}} = \infty)$ is simply the net mean transmission \bar{F} ; we also indicate \bar{F} from LUQAS, M00, FG and Kirkman et al. (2005).

For mock samples with ensemble average $\langle F \rangle = 0.79$ we find that the (continuum fitted) $\bar{F}(W_{\text{cut}} = \infty)$ varies between 0.79 and 0.84 within 2σ . Note that our procedure to estimate the errors due to ‘continuum fitting’ makes the mean transmission, \bar{F} systematically higher than $\langle F \rangle$. Observed determinations of the mean transmission are shown with horizontal lines in the figure. It appears that, despite the large dispersion amongst observed values, they are nevertheless consistent, because the expected sample variance, as inferred from GIMIC (and consistent with bootstrap estimates using real data for sufficiently large chunk size), is so large. The origin of the large variance is the presence of strong lines.

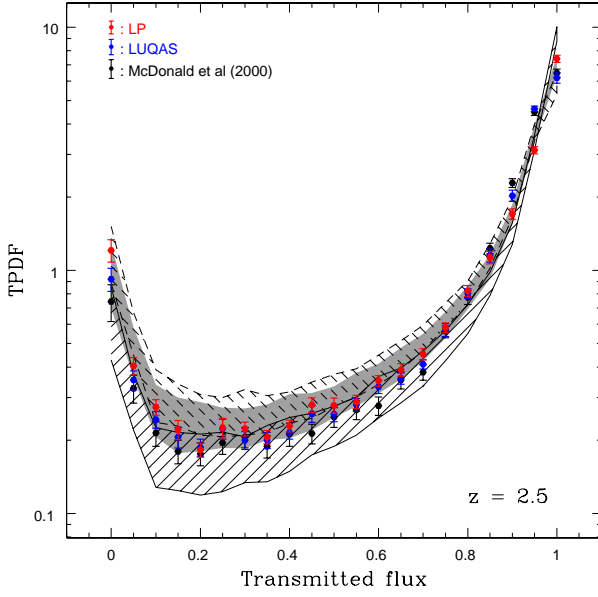


Figure 6. Dependence of the transmission PDF on the ensemble averaged $\langle F \rangle$ at $z = 2.5$. The dark shaded region shows the 2σ range computed from 400 mock samples in a GIMIC simulation with $\langle F \rangle = 0.77$ as in Fig. 3; Symbols with error bars are as in Fig. 3. Solid and dashed hashed regions correspond to the 2σ range in GIMIC simulations with $\langle F \rangle = 0.83$ and 0.74 , respectively. At these extremes the observational data (for transmission $0.1 < F < 0.7$) falls just outside the 2σ range of the simulation for at least one data point.

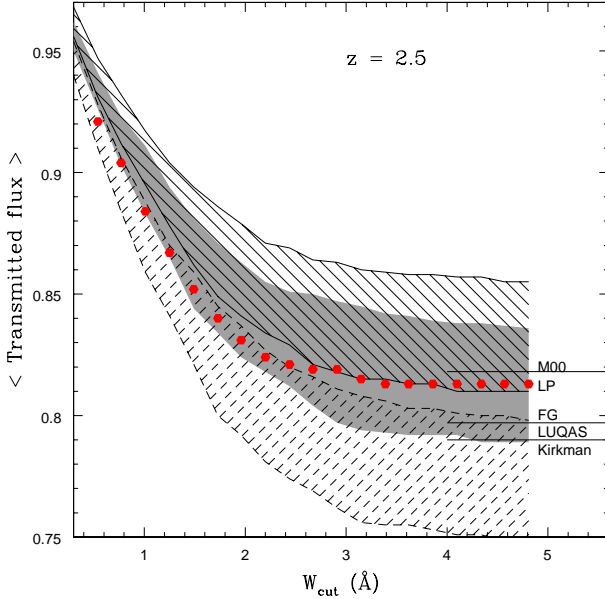


Figure 7. Same as Fig. 6, but for the dependence of the mean transmission as a function of maximum line width, $\bar{F}(W_{\text{cut}})$. Dark shaded region is the 2σ range for $\langle F \rangle = 0.79$, solid and dashed hashed regions correspond to the 2σ range in the GIMIC simulations with $\langle F \rangle = 0.81$ and 0.75 , respectively.

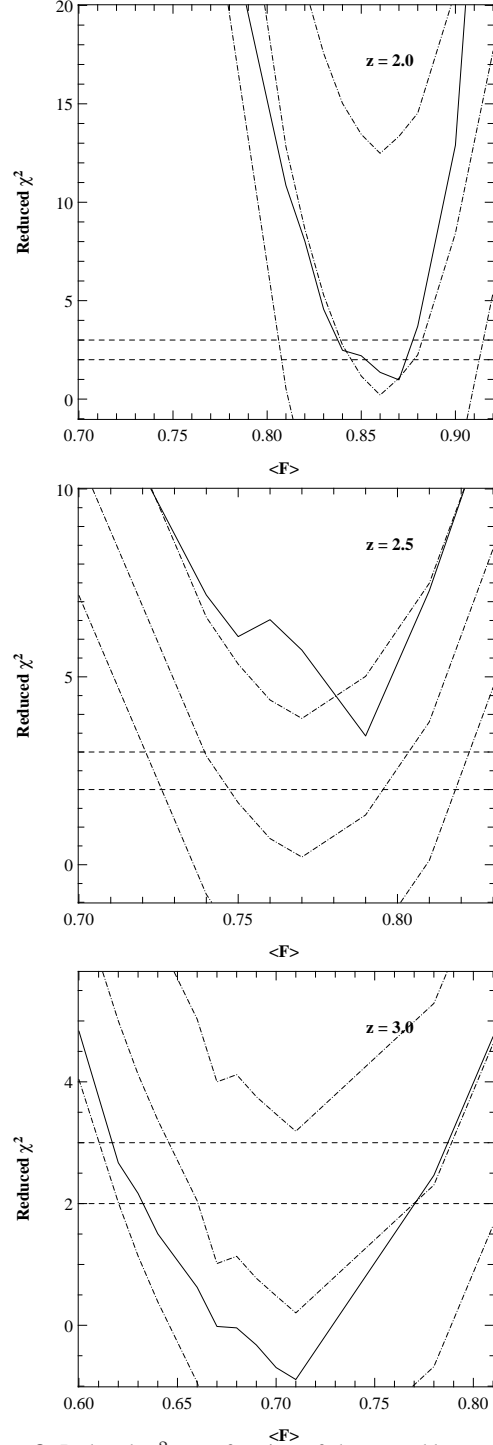


Figure 8. Reduced χ^2 as a function of the ensemble averaged $\langle F \rangle$ at $z = 2, 2.5, 3.0$ (top to bottom). The covariance matrix is measured using the variance among GIMIC mock samples. χ^2 corresponds to the difference between one TPDF and the averaged TPDF from 400 GIMIC mock samples assuming different $\langle F \rangle$. As a validity check, the TPDF measured in one GIMIC mock sample with $\langle F \rangle = 0.86, 0.77$ and 0.71 at $z = 2, 2.5, 3.0$ respectively, is best fitted with the same value for $\langle F \rangle$ (dotted lines show the average reduced χ^2 and the 1σ range among 400 samples). The evolution of the reduced χ^2 as a function of $\langle F \rangle$ is similar in the case of the observed LP (solid lines).

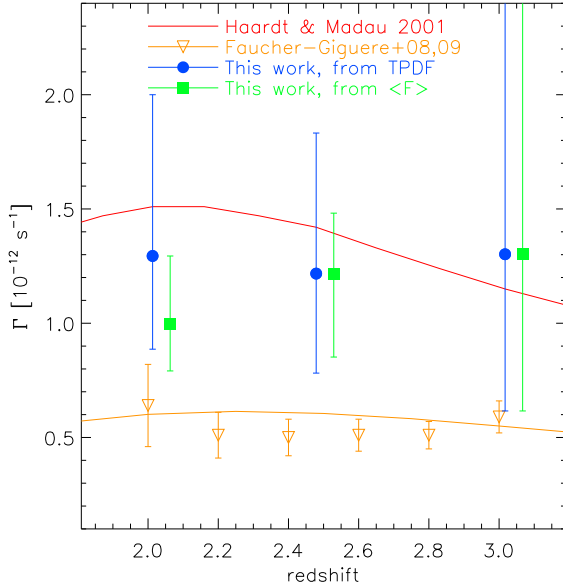


Figure 9. Mean hydrogen photo-ionization rate, Γ , as function of redshift, from summing over sources as computed by Haardt & Madau (2001, *red*) and Faucher-Giguère et al (2009, *drawn orange line*), and from comparing simulated to observed mock spectra. *Blue* and *green* points are our (2σ) determinations from comparing, respectively, the TPDF and the mean flux in the GIMIC simulations to the LP data, *orange* symbols are the Faucher-Giguère et al. (2008) determination using a sample of 84 high-resolution quasars.

Table 2. *Upper rows:* Measured value of the mean transmission in three redshift ranges for LUQAS and LP samples. Using the LP as a reference, the redshifts ranges are 1.88 – 2.37, 2.37 – 2.71, 2.71 – 3.21 with absorption distance of 10.3, 5.8 and 2.9 respectively. For LUQAS, Kim et al. (2007) provide errors computed by bootstrapping chunks of size 5\AA within bins of size $dz = 0.2$; their errors are then rescaled to the LP absorption distances. The errors given for LP correspond to the variance between GIMIC mock samples. *Lower rows:* ensemble-averaged $\langle F \rangle$ in GIMIC simulations that reproduce within 2σ the LP observed transmission PDF and mean transmission, \bar{F} ; the last row gives the ionising background rate values in the same GIMIC simulations. $\langle F \rangle$ refers to an ensemble average, \bar{F} refers to a single realisation of such an ensemble, and is generally larger than $\langle F \rangle$ because it includes a 2% continuum fitting offset.

$\bar{z} = 2.0$	$\bar{z} = 2.5$	$\bar{z} = 3.0$	
Measured \bar{F} ($\pm 2\sigma$)			
0.887 ± 0.011	0.812 ± 0.017	0.780 ± 0.034	LP
0.868 ± 0.010	0.775 ± 0.021	0.713 ± 0.032	LUQAS
Derived $\langle F \rangle$ with 2σ variance from GIMIC mocks.			
$0.86^{+0.007}_{-0.025}$	$0.77^{+0.005}_{-0.045}$	$0.71^{+0.06}_{-0.05}$	(from TPDF)
0.85 ± 0.02	$0.79^{+0.02}_{-0.04}$	$0.71^{+0.07}_{-0.09}$	(from \bar{F})
Derived Γ_{12} with 2σ range from GIMIC mocks.			
1.3 (0.9, 2.0)	1.2 (0.8, 1.8)	1.3 (0.6, 2.6)	

4 CONSTRAINTS ON THE MEAN TRANSMISSION AND THE INTENSITY OF THE IONISING BACKGROUND

The photo-ionization rate can be estimated by scaling mock spectra obtained from simulations to the observed mean transmission \bar{F} , and calculating the corresponding value of Γ_{12} . To determine the range of Γ_{12} values consistent with the observed \bar{F} , we need some measure of the expected variance of \bar{F} around its ensemble average $\langle F \rangle$. In principle, it should also be possible to use the full transmission PDF rather than just its mean.

To judge how well a given realisation of a mock transmission PDF fits an observational determination, one could use the usual χ^2 -estimator for values of the transmission between 0.1 and 0.7. A covariance matrix can be computed by cross-correlating estimates of the TPDF from a large number of bootstrap samples, as described in Lidz et al. (2006). Note that all bootstrap samples are then by construction sub-samples of the observed spectra, which limits their usefulness if the observed path length is small. When this is applied to the transmission PDF, it transpires that the covariance matrix is nearly singular and hence needs to be ‘regularized’ using a singular value decomposition. We found that the values obtained for χ^2 then depend strongly on the number of singular values regularised, which severely compromises the usual statistical interpretation of χ^2 . We can get around this problem by using the simulations to estimate the variance on either \bar{F} or the transmission PDF, for samples with given $\langle F \rangle$.

However, we have seen that the value of the mean transmission \bar{F} for a given realisation of a mock sample can differ considerably from the ensemble average $\langle F \rangle$ of the sample. Since the observations only provide a single measurement of \bar{F} , a potentially large range of ensemble averages are consistent with that \bar{F} . This is illustrated in Fig. 6 for the transmission PDF, and in Fig. 7 for \bar{F} , both at redshift $z = 2.5$. In both cases the dark grey band shows the 2σ range in mock samples drawn from simulations with a given value of the ensemble averaged transmission ($\langle F \rangle = 0.77$ and 0.79 respectively). As before, each sample has the same redshift path as the LP sample.

Considering first the mean transmission as a function of line-width, we demand the mean transmission with $W = \infty$ to fall within the 2σ region. We interpret these extreme values as 2σ limits on the ensemble average $\langle F \rangle$. The 2σ allowed range is then $0.75 \leq \langle F \rangle \leq 0.81$. As before, the determination of \bar{F} in the mock sample is done after ‘continuum fitting’, which implies that \bar{F} will be systematically higher than $\langle F \rangle$. Performing the same analysis at $z = 3$ and at $z = 2$, yields a 2σ allowed range of $0.62 \leq \langle F \rangle \leq 0.78$ and $0.83 \leq \langle F \rangle \leq 0.87$ respectively (Table 2).

To do a fit of the TPDF requires a measure of the covariance matrix. As explained above, data samples are not yet large enough to provide a reliable estimate of it. Rather, we compute the covariance using 400 independent determinations of the TPDF in GIMIC mock samples. The covariance matrix can thus be inverted without further regularization. We use 13 bins for a range of flux $0.1 < F < 0.7$, corresponding to $k = 12$ degree of freedoms. The evolution of the reduced $\chi^2_r = (\chi^2 - k)/\sqrt{2k}$ is shown in Fig. 8 (solid lines). To check the validity of this procedure, we derive the same evolution for different mock samples. Assuming a true value of $\langle F \rangle_{\text{true}}$ (0.71, 0.77 and 0.86 at $z = 2, 2.5$ and 3 respectively), we compare again 400 mock samples with different value of $\langle F \rangle$ to the average TPDF with $\langle F \rangle_{\text{true}}$, and compute the associated reduced χ^2_r . The average evolution of χ^2_r and its dispersion (dotted lines in Fig. 8) are consistent with the observed evolution using

the LP TPDF, despite a slight tension at $z = 2.5$. We provide a best fitting value and a 2σ range for $\langle F \rangle$ using the smooth average evolution in GIMIC samples: $0.845 \leq \langle F \rangle = 0.86 \leq 0.877$ at $z = 2.0$, $0.745 \leq \langle F \rangle = 0.77 \leq 0.795$ at $z = 2.5$ and $0.66 \leq \langle F \rangle = 0.71 \leq 0.77$ at $z = 3.0$. Note that the best fitting value for $\langle F \rangle$ is slightly shifted compared to the value corresponding to the observed minimum, in order to best reproduce the overall evolution of χ^2_r . Also, the range at $z = 2.5$ as determined from the evolution of χ^2 is narrower than the range determined by eye in Fig. 6. Those estimates for $\langle F \rangle$ and their 2σ uncertainty at these three redshifts can be compared to the values given in Table 2 that refer to the allowed range of $\langle F \rangle$ so that GIMIC simulations reproduce within 2σ the LP observed transmission PDF (Fig. 6). Our values are generally in agreement with previously published values, but our quoted uncertainties are significantly larger.

Given the constraints on $\langle F \rangle$, we can use the simulations to infer the corresponding range in photo-ionization rates $\Gamma(z)$, which, in addition to the inferred value of $\langle F \rangle$, depend on the baryon density, Ω_b , the temperature-density relation, the fluctuation amplitude σ_8 and other cosmological parameters (Rauch et al. 1997).

Our inferred values for the photo-ionization rate, $\Gamma(z)$, are compared in Fig. 9 to the results of Haardt & Madau (2001) and to those of Faucher-Giguère et al. (2008, 2009), and are also listed in Table 2. The red (Haardt & Madau 2001) and orange (Faucher-Giguère et al. 2009) curves combine observationally inferred values for the emissivities of sources of ionising photons with an assumed escape fraction and a model for the mean free path based on observations to estimate Γ . Note that Haardt & Madau (2011) derived recently a lower value of $\Gamma \simeq 0.9 \cdot 10^{-12} \text{ s}^{-1}$ for $2 < z < 3$. In agreement with these models, we find little evidence for evolution in Γ over the redshift range $z = 2-3$. This is also in agreement with the results of Bolton et al. (2005, , their Figure 7), although our error bars are again larger for $z = 2.5$ and 3. Our value for the amplitude is in good agreement with that from Haardt & Madau, but is a factor of ~ 2 larger than that of Faucher-Giguère et al. (2009). The latter value is not inferred from simulations, but from a fit to the density distribution of the IGM by Miralda-Escudé et al. (2000), itself guided by older simulations of Miralda-Escudé et al. (1996). The significant differences in cosmological parameters of those simulations might explain the significant offset in the inferred amplitude. Indeed, Pawlik et al. (2009) found that the Miralda-Escudé et al. fit did not describe their own simulations well.

5 DISCUSSION AND CONCLUSIONS

We have compared the mean transmission, \bar{F} , as well as the transmission probability distribution function, TPDF, in the H I Lyman- α forest as derived from several observational samples, as well as from mock samples computed using the GIMIC suite of hydrodynamical simulations. The mean transmission \bar{F} in the Lyman- α forest varies considerably from QSO to QSO, even at a given redshift. We have shown that, both in data and in simulations, this is due to the presence of strong lines, which, though relatively rare, contribute significantly to the opacity. This implies that a large redshift path is required to accurately determine the mean transmission.

We have compared in detail the variance σ on \bar{F} between published data, our own analysis of the observed UVES LP sample, and mocks computed from the GIMIC hydrodynamical simulations. We have shown, *from observations only*, that bootstrap errors

depend sensitively on chunk size, and only start to converge when relatively large chunks, $\gtrsim 25 \text{ \AA}$, are used. This is larger than typically used, and as a consequence we claim that published errors may be slightly underestimated, especially at larger redshift. We compared the mean transmission computed from the GIMIC simulations to that obtained from three observational samples. The GIMIC simulations are zoomed simulations of different density regions picked from the Millennium simulation, and as such they have a realistic amount of ‘sample variance’. We exploited this feature of the simulations to estimate the uncertainty in the determination of $\langle F \rangle$ for various observed samples. When we compute errors in the same way as performed in published work, we find excellent agreement between published and predicted values. We have also shown that converged bootstrap errors are in good agreement with errors found from bootstrapping *mock samples*. Thus, we find larger uncertainties than in previous works. For a given value of $\langle F \rangle$, the variance on the mean transmission is large enough to make all previously published values consistent within the scatter.

Using mock spectra derived from GIMIC, we have investigated the dependence of the variance of the mean transmitted flux on the absorption path ΔX , see Table 3. At $z = 2.5$, with a sample twice as large as the LP sample, the 2σ variance is only 0.013 and decreases down to 0.009 with a sample four times as large, which is half of the value for 2σ for one LP sample, as expected. We note, however, that the size of our simulations may not be sufficient to evaluate the variance with such a large velocity path, especially at $z = 2$.

We have also investigated the probability distribution of the transmission. The ensemble variance between mock samples is systematically larger than the jack-knife errors used by previous authors, by a factor of 1.5–2 in the redshift bins $\bar{z} = 3$. More importantly, the covariance matrix derived from a suite of mocks can be inverted without regularization, contrary to standard estimate with jack-knife methods. We used these larger errors and compare data to simulations.

The temperature-density relation, $T = T_0 (\rho/\langle\rho\rangle)^{\gamma-1}$, in the GIMIC simulations is a result of adiabatic cooling and photo-heating due to an imposed ionising-background as computed by Haardt & Madau (2001), tweaked to yield values for T_0 and γ consistent with the measured values of Schaye et al. (2000). In this model $\gamma > 1$ at all times, with a minimum value of $\gamma \simeq 1.3$ around redshift $z = 3$ caused by HeII re-ionization (Theuns et al. 2002). The GIMIC transmission PDF is in agreement with that measured from high-resolution quasar spectra over the redshift range $z = 2-3$ in the transmission range $0.1 < F < 0.7$. For $F < 0.1$ there may be differences due to the neglect of self-shielding in the simulations, whereas for $F > 0.7$ uncertainties in continuum fitting the data complicate the comparison. This agreement is obtained using a specific set of cosmological parameters. In particular, we assume $\sigma_8 = 0.9$. The goal of this work is not to provide the best fitting cosmological model, but to point out the large effect of sample variance. Indeed, our model with $(\sigma_8, \gamma) = (0.9, 1)$ is not ruled out by the current set of data, while Viel et al. (2009) discard those values at more than 2σ when considering the whole flux range. Thus, we argue that previous suggestions for an inverted T - ρ relation may have resulted from an underestimate of the errors in the observations, rather than a discrepancy between data and the standard model.

Table 3. Dependence of the variance of the mean transmission on absorption distance ΔX , for three redshifts. The top row shows the variance (2σ) for the current LP sample (with given absorption distance ΔX LP). The second and third rows are for samples two, and four times as large. Errors correspond to the variance among mock LP samples.

ΔX LP	$\bar{z} = 2.0$ 10.5	$\bar{z} = 2.5$ 5.8	$\bar{z} = 3.0$ 2.9	sample size
	0.011	0.017	0.034	$\Delta X \times 1$
	0.0078	0.013	0.024	$\Delta X \times 2$
	0.0054	0.0088	0.017	$\Delta X \times 4$

ACKNOWLEDGEMENTS

We thank the anonymous referee for useful comments that improved the quality of the paper. We would like to thank our collaborators to allow us to analyse the GIMIC simulations for this purpose. These simulations were carried out using the HPCx facility at the Edinburgh Parallel Computing Centre (EPCC) as part of the EC's DEISA 'Extreme Computing Initiative', and with the Cosmology Machine at the Institute for Computational Cosmology of Durham University. This work was supported by an NWO VIDI grant and by the Marie Curie Initial training Network CosmoComp (PITN-GA-2009-238536).

REFERENCES

Altay G., Theuns T., Schaye J., Crighton N. H. M., Dalla Vecchia C., 2011, *ApJ*, 737, L37
 Aracil B., Petitjean P., Pichon C., Bergeron J., 2004, *A&A*, 419, 811
 Becker G. D., Bolton J. S., Haehnelt M. G., Sargent W. L. W., 2011, *MNRAS*, 410, 1096
 Becker G. D., Rauch M., Sargent W. L. W., 2007, *ApJ*, 662, 72
 Bergeron J., Petitjean P., Aracil B. *et al.*, 2004, *The Messenger*, 118, 40
 Bi H. G., Boerner G., Chu Y., 1992, *A&A*, 266, 1
 Bolton J. S., Haehnelt M. G., Viel M., Springel V., 2005, *MNRAS*, 357, 1178
 Bolton J. S., Oh S. P., Furlanetto S. R., 2009, *MNRAS*, 395, 736
 Bolton J. S., Viel M., Kim T.-S., Haehnelt M. G., Carswell R. F., 2008, *MNRAS*, 386, 1131
 Boyarsky A., Ruchayskiy O., Iakubovskiy D., 2009, *Journal of Cosmology and Astro-Particle Physics*, 3, 5
 Calura F., Tescari E., D'Odorico V., Viel M., Cristiani S., Kim T.-S., Bolton J. S., 2012, *MNRAS*, 422, 3019
 Carswell R. F., Webb J. K., Baldwin J. A., Atwood B., 1987, *ApJ*, 319, 709
 Cen R., Miralda-Escudé J., Ostriker J. P., Rauch M., 1994, *ApJ*, 437, L9
 Chang P., Broderick A. E., Pfrommer C., 2011, *ArXiv:astro-ph/1106.5504*
 Cowie L. L., Songaila A., Kim T.-S., Hu E. M., 1995, *AJ*, 109, 1522
 Crain R. A., Theuns T., Dalla Vecchia C. *et al.*, 2009, *MNRAS*, 399, 1773
 Crighton N. H. M., Morris S. L., Bechtold J., Crain R. A., Jannuzi B. T., Shone A., Theuns T., 2010, *MNRAS*, 402, 1273
 Dalla Vecchia C., Schaye J., 2008, *MNRAS*, 387, 1431
 Desjacques V., Nusser A., Sheth R. K., 2007, *MNRAS*, 374, 206

Fan X., Carilli C. L., Keating B., 2006, *ARA&A*, 44, 415
 Faucher-Giguère C., Lidz A., Zaldarriaga M., Hernquist L., 2009, *ApJ*, 703, 1416
 Faucher-Giguère C.-A., Prochaska J. X., Lidz A., Hernquist L., Zaldarriaga M., 2008, *ApJ*, 681, 831
 Fukugita M., Hogan C. J., Peebles P. J. E., 1998, *ApJ*, 503, 518
 Gratton S., Lewis A., Efstathiou G., 2008, *Physical Review D*, 77, 083507
 Guimarães R., Petitjean P., Rollinde E., de Carvalho R. R., Djorgovski S. G., Srianand R., Aghaee A., Castro S., 2007, *MNRAS*, 377, 657
 Gunn J. E., Peterson B. A., 1965, *ApJ*, 142, 1633
 Haardt F., Madau P., 2001, in Neumann D. M., Tran J. T. V., eds, *Clusters of Galaxies and the High Redshift Universe Observed in X-rays Modelling the UV/X-ray cosmic background with CUBA*
 Haardt F., Madau P., 2011, *ArXiv:1105.2039*
 Hernquist L., Katz N., Weinberg D. H., Miralda-Escudé J., 1996, *ApJ*, 457, L51
 Hu E. M., Kim T.-S., Cowie L. L., Songaila A., Rauch M., 1995, *AJ*, 110, 1526
 Hui L., Gnedin N. Y., 1997, *MNRAS*, 292, 27
 Hui L., Haimes Z., 2003, *ApJ*, 596, 9
 Kim T.-S., Bolton J. S., Viel M., Haehnelt M. G., Carswell R. F., 2007, *MNRAS*, 382, 1657
 Kim Y.-R., Croft R. A. C., 2008, *MNRAS*, 387, 377
 Kirkman D., Tytler D., Suzuki N., Melis C., Hollywood S., James K., So G., Lubin D., Jena T., Norman M. L., Paschos P., 2005, *MNRAS*, 360, 1373
 Komatsu E., Dunkley J., Nolte M. R., Bennett C. L., Gold B., Hinshaw G., Jarosik N., Larson D., Limon M., Page L., Spergel D. N., Halpern M., Hill R. S., Kogut A., Meyer S. S., Tucker G. S., Weiland J. L., Wollack E., Wright E. L., 2009, *ApJS*, 180, 330
 Lidz A., Faucher-Giguère C.-A., Dall'Aglio A., McQuinn M., Fechner C., Zaldarriaga M., Hernquist L., Dutta S., 2010, *ApJ*, 718, 199
 Lidz A., Heitmann K., Hui L., Habib S., Rauch M., Sargent W. L. W., 2006, *ApJ*, 638, 27
 Lynds R., 1971, *ApJ*, 164, L73
 McDonald P., Miralda-Escudé J., 1999, *ApJ*, 518, 24
 McDonald P., Miralda-Escudé J., Rauch M. *et al.*, 2000, *ApJ*, 543, 1
 McDonald P., Miralda-Escudé J., Rauch M., Sargent W. L. W., Barlow T. A., Cen R., 2001, *ApJ*, 562, 52
 McDonald P., Seljak U., Burles *et al.*, 2006, *ApJS*, 163, 80
 McDonald P., Seljak U., Cen R., Bode P., Ostriker J. P., 2005, *MNRAS*, 360, 1471
 McQuinn M., Hernquist L., Lidz A., Zaldarriaga M., 2011, *MNRAS*, 415, 977
 McQuinn M., Lidz A., Zaldarriaga M., Hernquist L., Hopkins P. F., Dutta S., Faucher-Giguère C.-A., 2009, *ApJ*, 694, 842
 Meiksin A., Bryan G., Machacek M., 2001, *MNRAS*, 327, 296
 Miralda-Escudé J., Cen R., Ostriker J. P., Rauch M., 1996, *ApJ*, 471, 582
 Miralda-Escudé J., Haehnelt M., Rees M. J., 2000, *ApJ*, 530, 1
 Mortlock D. J., Warren S. J., Venemans B. P., Patel M., Hewett P. C., McMahon R. G., Simpson C., Theuns T., González-Solares E. A., Adamson A., Dye S., Hambly N. C., Hirst P., Irwin M. J., Kuiper E., Lawrence A., Röttgering H. J. A., 2011, *Nature*, 474, 616
 Pawlik A. H., Schaye J., van Scherpenzeel E., 2009, *MNRAS*, 394, 1812

- Petitjean P., Mueket J. P., Kates R. E., 1995, *A&A*, 295, L9
- Petitjean P., Webb J. K., Rauch M., Carswell R. F., Lanzetta K., 1993, *MNRAS*, 262, 499
- Puchwein E., Pfrommer C., Springel V., Broderick A. E., Chang P., 2011, *ArXiv:astro-ph/1107.3837*
- Rauch M., 1998, *ARA&A*, 36, 267
- Rauch M., Miralda-Escude J., Sargent W. L. W., Barlow T. A., Weinberg D. H., Hernquist L., Katz N., Cen R., Ostriker J. P., 1997, *ApJ*, 489, 7
- Ricotti M., Gnedin N. Y., Shull J. M., 2000, *ApJ*, 534, 41
- Rollinde E., Petitjean P., Pichon C., Colombi S., Aracil B., D’Odorico V., Haehnelt M. G., 2003, *MNRAS*, 341, 1279
- Rollinde E., Srianand R., Theuns T., Petitjean P., Chand H., 2005, *MNRAS*, 361, 1015
- Schaye J., 2001, *ApJ*, 559, 507
- Schaye J., Aguirre A., Kim T.-S., Theuns T., Rauch M., Sargent W. L. W., 2003, *ApJ*, 596, 768
- Schaye J., Dalla Vecchia C., 2008, *MNRAS*, 383, 1210
- Schaye J., Dalla Vecchia C., Booth C. M., Wiersma R. P. C., Theuns T., Haas M. R., Bertone S., Duffy A. R., McCarthy I. G., van de Voort F., 2010, *MNRAS*, 402, 1536
- Schaye J., Theuns T., Rauch M., Efstathiou G., Sargent W. L. W., 2000, *MNRAS*, 318, 817
- Springel V., 2005, *MNRAS*, 364, 1105
- Springel V., White S. D. M., Jenkins A., Frenk C. S., Yoshida N., Gao L., Navarro J., Thacker R., Croton D., Helly J., Peacock J. A., Cole S., Thomas P., Couchman H., Evrard A., Colberg J., Pearce F., 2005, *Nature*, 435, 629
- Theuns T., Leonard A., Efstathiou G., Pearce F. R., Thomas P. A., 1998, *MNRAS*, 301, 478
- Theuns T., Schaye J., Zaroubi S., Kim T.-S., Tzanavaris P., Carswell B., 2002, *ApJ*, 567, L103
- Theuns T., Viel M., Kay S., Schaye J., Carswell R. F., Tzanavaris P., 2002, *ApJ*, 578, L5
- Theuns T., Zaroubi S., Kim T.-S., Tzanavaris P., Carswell R. F., 2002, *MNRAS*, 332, 367
- Tytler D., Paschos P., Kirkman D., Norman M. L., Jena T., 2009, *MNRAS*, 393, 723
- Viel M., Bolton J. S., Haehnelt M. G., 2009, *MNRAS*, 399, L39
- Viel M., Haehnelt M. G., 2006, *MNRAS*, 365, 231
- Viel M., Haehnelt M. G., Carswell R. F., Kim T.-S., 2004, *MNRAS*, 349, L33
- Wiersma R. P. C., Schaye J., Smith B. D., 2009, *MNRAS*, 393, 99
- Wiersma R. P. C., Schaye J., Theuns T., Dalla Vecchia C., Tomatore L., 2009, *MNRAS*, 399, 574
- Zhang Y., Anninos P., Norman M. L., 1995, *ApJ*, 453, L57